symmetry

MDPI

Article

Development of a Computer System for Automatically Generating a Laser Photocoagulation Plan to Improve the Retinal Coagulation Quality in the Treatment of Diabetic Retinopathy

Nataly Ilyasova [1], Nikita Demin [1] and Nikita Andriyanov [2,*]

[1] Image Processing Systems Institute of the Russian Academy of Sciences, Branch of the Federal Scientific Research Centre "Crystallography and Photonics" RAS, Molodogvardeyskay, 151, 443001 Samara, Russia
[2] Data Analysis and Machine Learning Department, Financial University under the Government of the Russian Federation, Leningradsky pr-t, 49, 125167 Moscow, Russia
* Correspondence: naandriyanov@fa.ru; Tel.: +7-(499)-503-4700

Abstract: In this article, the development of a computer system for high-tech medical uses in ophthalmology is proposed. An overview of the main methods and algorithms that formed the basis of the coagulation plan planning system is presented. The system provides the formation of a more effective plan for laser coagulation in comparison with the use of existing coagulation techniques. An analysis of monopulse- and pattern-based laser coagulation techniques in the treatment of diabetic retinopathy has shown that modern treatment methods do not provide the required efficacy of medical laser coagulation procedures, as the laser energy is nonuniformly distributed across the pigment epithelium and may exert an excessive effect on parts of the retina and anatomical elements. The analysis has shown that the efficacy of retinal laser coagulation for the treatment of diabetic retinopathy is determined by the relative position of coagulates and parameters of laser exposure. In the course of the development of the computer system proposed herein, main stages of processing diagnostic data were identified. They are as follows: the allocation of the laser exposure zone, the evaluation of laser pulse parameters that would be safe for the fundus, mapping a coagulation plan in the laser exposure zone, followed by the analysis of the generated plan for predicting the therapeutic effect. In the course of the study, it was found that the developed algorithms for placing coagulates in the area of laser exposure provide a more uniform distribution of laser energy across the pigment epithelium when compared to monopulse- and pattern-based laser coagulation techniques.

Keywords: fundus; laser coagulation; diabetic retinopathy; image processing; segmentation; classification

Citation: Ilyasova, N.; Demin, N.; Andriyanov, N. Development of a Computer System for Automatically Generating a Laser Photocoagulation Plan to Improve the Retinal Coagulation Quality in the Treatment of Diabetic Retinopathy. *Symmetry* **2023**, *15*, 287. https://doi.org/10.3390/sym15020287

Academic Editor: José Carlos R. Alcantud

Received: 15 November 2022
Revised: 10 January 2023
Accepted: 16 January 2023
Published: 20 January 2023

1. Introduction

Recently, the introduction of artificial intelligence and digital medicine technologies into healthcare practice is rapidly changing the methods of diagnosis and treatment [1–8]. Robotic systems are used to support the diagnosis and treatment of diseases [9–13]. Ophthalmology is in dire need of the development and implementation of fundamentally new intelligent methods for analyzing the biomedical data of patients [14–16].

Diabetes mellitus (DM) is a common endocrine disease affecting all human organs [17]. Diabetic retinopathy (DR) is a manifestation of the disease on the visual apparatus [18,19]. Today, there are almost 400 million patients with DM in the world, and the number is expected to increase to 600 million people by 2040 [20]. The most dangerous manifestation of DR is diabetic macular edema (DME). The walls of retinal vessels become thinner and hemorrhages occur in the retinal area, leading to partial or complete loss of vision [21–23]. According to the Wisconsin Epidemiological Study of Diabetic Retinopathy (WESDR) [24], after 20 years of diabetes, retinopathy is detected in 80–100% of cases, while DME develops in 29% of cases.

In modern medical practice, DR is a common disease that leads to the development of pathological elements in the fundus, including exudates, macular edema, retinal hemorrhages, and newly formed vessels [25–27]. Laser coagulation is used for the treatment of DR [28–33]. During laser coagulation, certain areas of the retina are exposed to laser impact to prevent macular edema [34–37].

On the world market, modern systems for the treatment of diabetic retinopathy do not provide sufficient efficacy of laser coagulation, so rather than guiding the laser beam manually, the experienced ophthalmologists prefer to rely upon a preformed coagulation plan [38–40]. The most modern device is NAVILAS [35,41–43]. It was developed by the German company ODOS, and NAVILAS provides automatic laser guidance according to the formed coagulation plan, while the coagulation plan is created manually based on the selection of the laser exposure zone and the hexagonal method of coagulates location in this zone. However, experienced medical doctors are uncomfortable with this approach [35,44–46] and often return to using older treatment methods, for example, VALON equipment, which supports the patterned laser coagulation technique [47].

High efficacy in the treatment of diabetic retinopathy can be achieved using an augmented reality system in conjunction with an appropriate device, such as VALON. The most convenient augmented reality system can be based on the implementation of a translucent display in an appropriate device, which, on the one hand, can display the coagulation plan, and, on the other hand, the surgeon using such a system can see the real retina. Thus, the device assumes the presence of a fundus camera for processing the image of the fundus on the workstation, a translucent display on which the coagulation plan is displayed over the visible fundus, sensors that determine the coordinates of the laser, and appropriate mirrors so that the fundus camera does not interfere with the translucent display. A simpler system includes just a conventional fundus camera and a small monitor on which the fundus image and processing results are displayed. The NAVILAS system supports the ability to combine an image with the result of DR treatment planning, which can also be used instead of an augmented reality system. This approach is aimed at significantly increasing the efficacy of laser coagulation treatment [35,41,44,47–49].

The main problem is the lack of a method for automatically generating a coagulation plan, that is, a software system that could process the fundus images and create a laser coagulation plan. Such system now is only under development using modern programming languages. Most importantly, the generated coagulation plan needs to meet a requirement of safe treatment, with laser radiation possibly not damaging the retina, nor affecting the prohibited areas. In addition, the plan must ensure an even distribution of energy across the pigment epithelium in order to achieve a maximum therapeutic effect. First of all, it is necessary to select the parameters of laser exposure so that the result of coagulation does not lead to adverse effects. At the moment, the minimum distance between coagulates, the radius of point coagulation, and the parameters of laser exposure are selected empirically based on the experience from previous surgical procedures [44,50]. In the NAVILAS, the minimum distance between coagulates is set by default with a margin, but the surgeon can correct this plan [41]. The same applies to the parameters of laser exposure, such as pulse duration, power, time between adjacent shots. In ophthalmology, there is no non-invasive way to evaluate safe parameters of laser exposure [44,47,48,51,52]. However, it is possible to obtain information about the condition of the fundus using non-invasive methods. Optical coherence tomography (OCT) allows for the formation of a three-dimensional structure of the fundus, using which the surgeon first of all pays attention to the retinal thickness and its deviation from the normal thickness. When using a three-dimensional structure of the fundus, the parameters of laser exposure can be determined based on the mathematical modeling of fundus exposure to laser light [53–55].

Once the parameters of safe laser coagulation have been known, it is necessary to determine which zone can be exposed to laser pulses, as well as which zone is pathological and should be coagulated [44,47,48,56]. To form a coagulation plan, it is necessary to perform two key steps: identifying the area of laser exposure that needs to be coagulated [57–73] and

forming a coagulation plan in the selected area [74,75]. To isolate the area of laser exposure, it is necessary to apply a set of methods [69–72] for the automatic formation of a binary image with a laser impact zone. To guarantee safety, the system should provide the medical doctor with the opportunity to correct the laser exposure area.

At the second stage, algorithms should be applied that primarily ensure safety in terms of the minimum distance between the coagulate centers [74–76]. In addition, the area of point coagulation should be strictly inside the zone of laser exposure. These conditions must be satisfied by any algorithm for applying coagulates. The main task that needs to be solved using coagulate placement algorithms is to increase the efficiency of the coagulation plan [54,77–79]. So far, there are no works devoted to the automatic formation of a coagulation plan according to patient data. In [35], the authors proposed a method based on the manual planning of coagulates, taking into account the pathological and anatomical areas of the fundus. In works [35,47], the coagulation plan was shown to affect the therapeutic effect. Despite the existence of a large number of digital methods for diagnosing DR [59–68,80] and methods for identifying anatomical and pathological zones [69–72], the task of automatically generating a coagulation plan within the selected zone has not been previously considered, remaining relevant to date.

The purpose of this work is to develop a computer system for high-tech medical uses in ophthalmology that would improve the efficacy of laser coagulation therapy for DR. To achieve this goal, the following tasks are solved: analysis of monopulse- and pattern-based methods for the treatment of DR based on retinal laser coagulation [78], identification of the diagnostic data processing stages for the formation and intellectual analysis of a preliminary coagulation plan [77]; development of mathematical models of the fundus to describe the state of the retina, a vascular layer, and pathological and anatomical elements in the fundus and the coagulation process [79]; development of an algorithm for assessing safe laser exposure parameters based on numerical methods for laser coagulation mathematical modeling [54,81–83]; development of algorithms for the automatic formation of a preliminary coagulation plan in the laser exposure zone using effective parameters of point coagulation [74,75]; development of a method for assessing the quality of a laser coagulation plan using data mining methods [84]; development of methodological, algorithmic base and software for the formation of a recommended laser coagulation strategy for the DR treatment and decision support for an ophthalmologist.

We set ourselves a goal of providing ophthalmic surgeons with an intelligent system that would offer a recommended treatment plan using individual patient data in a matter of a few seconds just prior to the surgical procedure. The smart system discussed in this paper will allow doctors to monitor the recommended treatment plan for diabetic retinopathy in a real time mode.

2. Digital Methods for Analyzing Fundus Data

The fundus, mathematical models of blood vessels and the optic nerve head are used to solve problems of diagnosing DR [81–94]. Works [41,44,47,48] are devoted to improving the quality of DR treatment and based on selecting an appropriate method for applying coagulates. These medical works are aimed at studying various methods of applying the coagulates manually, while taking into account anatomical factors. In this case, digital methods for isolating pathological and anatomical areas of the fundus can be used to support the formation of a coagulation plan by a medical doctor [35,86,95]. The majority of works that deal with the problem of identifying pathological and anatomical elements in fundus images are aimed at diagnosing DR [89,91–94]. For example, articles by Hervella A.S. [89] and Akram M.U. [90] aimed to highlight blood vessels in the image of the fundus. These works are based on the use of image processing methods, such as rank filtering, adaptive thresholding, calculation of texture features in the vicinity of pixels, and morphological methods. The disadvantage of using texture features is the high computational complexity. It can take over 20 min to segment a standard-size image. There are works on assessing vascular parameters, thanks to which the severity of DR is

assessed [82,83,85,96–100]. For example, article [100] presents a vascular tracing method for assessing tortuosity and calculating geometric and textural features to classify stages of the disease. Tree and spatial models of blood vessels for the heart and fundus were discussed in the work. Geometric features calculated using these models have made it possible to classify the vascular system and assess the degree of retinal damage [83,98–100]. The advantage of the method is that it enables the vessel tortuosity to be evaluated in a very short period of time, but on the negative side is the need to identify the starting and end points of each vessel. The method considered in [100] involves manual marking of key points of the vascular system.

Song Guo, Moazam Fraz and Worapan Kusakunniran proposed specific methods for identifying exudation zones in the fundus image [57–59]. The selection of exudates is most often based on selecting bright areas and analyzing the geometry of the selected zones. Approaches based on the use of texture features in the analysis of the green channel and HSV channels, perceptrons and decision trees, on the one hand, lead to high accuracy at the level of 99% but on the other hand, to high computation time, which is a key disadvantage. Authors who prefer machine learning provide results within 300 ms, which is an important advantage. The works by Ananyin, Ilyasova and Kupriyanov [81,101] are devoted to the isolation of the optic disc and the fovea using geometric parameters. The local fan-shaped transformation and geometric features were used as the main tools for solving this problem. The optic disc is oval in shape. The above-mentioned works focused on constructing an ellipse describing the optic disc. The advantage of this approach is the high-speed performance.

Isolation of edema zones in a fundus image is a separate task, which was studied in medical articles by Ramani [61] and Silverstein [102]. The scientists studied forms of edema, as well as the structure of pathological areas in the macular region in the fundus image under various disease conditions. In both works, the emphasis was placed on the possibility of segmentation of pathological areas in the fundus image. Edema zones are identified using either textural features [103–105], or convolutional neural networks [3,10,106,107]. The use of texture features and a sliding window for image segmentation leads to serious computational costs. The key advantage that convolutional neural networks provide is the short segmentation time. In [108], we showed that convolutional neural networks are better suited than textural features for solving the problem of identifying pathological and anatomical zones in the fundus image.

All over the world, a task of segmentation of OCT images aimed at isolating retinal layers remains a topical issue. At the moment, segmentation is carried out on the basis of the use of convolutional neural networks. Sandra Morales and Yufan He use the U-net network for layer segmentation [67,68]. Segmented layers can be used to form a layer thickness map. Thanks to the analysis of OCT images, a fundus structure is formed, which complements the information provided by the fundus image. This information is actively used to analyze the state of the retina in terms of pathological and anatomical features that can only be observed using OCT.

Research on laser coagulation effectiveness has been under way for over 10 years. Particular attention is paid to the evaluation of laser impact parameters [35,109–114]. At the moment, the parameters are subjectively chosen. Then, the dependences of the effective parameters of exposure on the features of the fundus are studied. In [35], an analysis was made of the relative position of coagulates and the therapeutic effect following laser coagulation. In that publication, the experts concluded that the most effective coagulation plan was a uniform plan in which inter-coagulate distances were possibly the same, that is, the smaller the standard deviation, the more uniform the plan. The disadvantage of the approaches described in the above-mentioned medical articles is the high error. Meanwhile, a highly accurate visual assessment of safe parameters of laser exposure during laser coagulation is problematic.

The evaluation of laser radiation parameters is a very important task, but doctors set the parameters subjectively based on their experience. Safe parameters can be automatically

assessed on the basis of mathematical modeling of the exposure of the fundus to laser light. In [53], modeling was carried out for Nd:YAG, ArF Excimer, and Nd:YAP lasers, which are designed to correct the visual acuity or apply drastic methods for treating the severely damaged retina. However, these types of lasers are not suitable for laser coagulation in the treatment of DR [115]. In addition, in [53] an ideal model of the eye was built, and in order to form safe parameters, it was suggested that an analysis should be conducted of fundus structures of real patients with retinal impairment (individual structure of the retina with a high thickness in the area of edema, individual shape of the epithelium layer, specific blood vessels).

Techniques based on the automatic formation of a coagulation plan in the area of laser exposure have not been previously proposed. For the task to be formally described, conditions for the effectiveness of the coagulation plan need to be determined. The conditions are formed on the basis of data mining [116–123] based on which a study of the feature space is carried out, and, if possible, informative features are selected, and factors that affect the accuracy of determining the data categories under study are identified. A preliminary coagulation plan can be described by a set of features by which the effectiveness of the plan is evaluated. In the simplest case, the estimated parameters can be used to evaluate the probability of the successful operation outcome. Such an assessment requires a large patient database. In modern medical practice, the therapeutic effect of laser exposure is not predicted. Instead, ophthalmologists empirically select a treatment technique and evaluate characteristics of the plan, according to which they prognosticate the effectiveness of laser coagulation [35].

3. System for Automatic Laser Coagulation Plan Formation

This article proposes a technology that includes methods for processing fundus images, automatic formation of a coagulation plan, and intellectual analysis of the generated coagulation plans for further prediction of the therapeutic effect (Figure 1). The system includes the following main steps:

1. Allocation of the laser impact zone based on the result of semantic segmentation and allocation of the pathological zone using OCT data;
2. Automatic planning of coagulation in the selected area;
3. Intelligent analysis of the generated coagulation plan to predict the therapeutic effect.

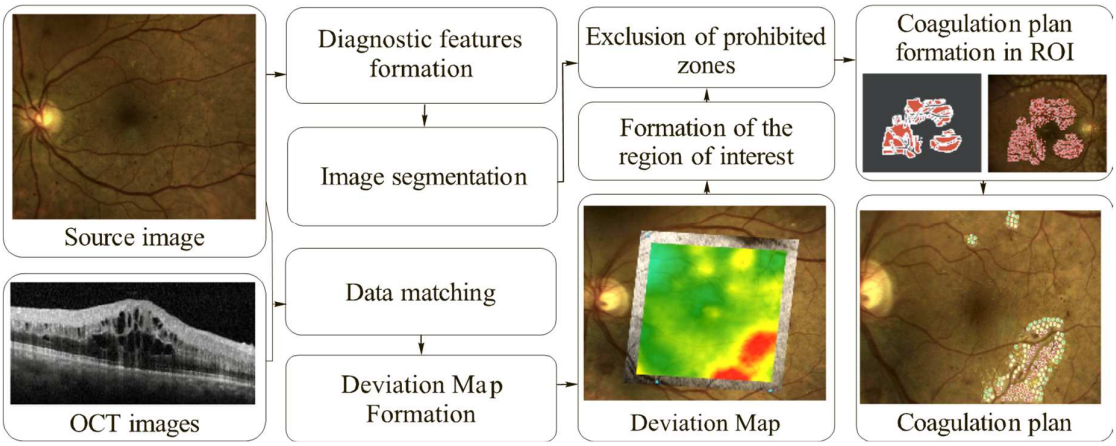

Figure 1. Technology of mapping a laser photocoagulation plan.

Segmentation of the fundus image involves selecting pathological and anatomical features in the image that are necessary to identify zones prohibited from laser exposure to prevent negative side-effects from coagulation. Such zones are excluded from the pathological zone, which is an area with the abnormal retinal structure. Modern ophthalmological programs for OCT use tools of highlighting the pathological zone.

When planning a coagulate pattern, many factors should be taken into account, but the key approach to the effective planning is attaining a uniform distribution of coagulates across the selected area [35]. Safe treatment implies that the inter-coagulate distance should not exceed a predetermined, safe distance. When implementing the coagulation plan, it is also necessary to take into account parameters of laser exposure, which ophthalmologists currently evaluate based on their subjective personal assessment.

Prior to implementing the created coagulation plan, it needs to be analyzed. Some outcomes of laser treatment can be predicted based on the formed plan. For example, if any area is not filled optimally, then the effectiveness of laser coagulation will be reduced. A number of studies [35,41,44,47,48] have shown that the therapeutic effect can be predicted from distances between the coagulates. Thus, the task of identifying criteria for assessing the coagulation plan quality and methods for predicting the therapeutic effect based on the generated plan is relevant. In [84], we proposed an approach for assessing the quality of a laser coagulation plan. The approach provides methods for calculating features, extracting the informative features, and predicting the therapeutic effect [84].

Estimates of safe laser coagulation obtained by numerical simulation [54] are used to automatically form a uniform coagulation plan, with the automatic formation being possible if there is a minimum distance between centers of the coagulates. In [35], authors showed the uniform coagulation plan to provide a higher efficacy compared to a monopulse technique currently employed in medical practice. Coagulates should maximally cover all zones of laser exposure, with the inter-coagulate distance being approximately the same.

In the course of research, a method for automatically mapping a laser coagulation plan was developed to improve its quality in the treatment of DR. Solving the problem of the automatic formation of a coagulation plan requires the use of quantitative characteristics of the effectiveness of the DR treatment. In medical practice, the effectiveness of treatment is a very subjective notion based on which medical doctors use different hypotheses that allow them to evaluate numerical indicators for specific diseases, according to which a specialist evaluates the effectiveness of treatment. For example, in [35], experts demonstrated the effectiveness of the treatment of DR to mainly depend on the effectiveness of the coagulation plan, that is, on the relative position of coagulates and parameters of point laser effects. In modern practice, doctors mainly use manual methods of applying coagulates to the fundus. Laser coagulation according to a preliminary, effective coagulation plan allows for treatment to be carried out more effectively than existing methods [35]. When using the most modern system NAVILAS, the surgeon needs to manually form the coagulation plan immediately before the laser treatment, which leads to a number of inconveniences [112]. The main advantage of the system is automatic laser guidance according to the generated plan. Automatic laser guidance does not provide sufficient efficacy of laser treatment of DR as this approach does not take into account all pathological and anatomical features of the fundus [47]. Of greatest interest is the automatic formation of the coagulation plan since the manual formation requires a long time to achieve the highest efficacy.

Automatic formation of a coagulation plan should be based on safety requirements and high treatment efficacy. Such requirements were mentioned above. The most preferable requirements include the optimal location of coagulates in the zone of macular edema at possibly equal distances from each other and the exclusion of their contact with blood vessels. If the placement of coagulates is performed manually according to one of these criteria, then the optimal location will be subjective, and more time will be spent on planning [35,124]. To automate the procedure of laser coagulation, the zone of laser exposure needs to be selected at the first stage. At the second stage, coagulates are placed in the zone of laser exposure.

3.1. Isolation of the Laser Impact Zone in the Fundus Images

At the first stage of the proposed method for automatically generating a coagulation plan, a laser exposure zone is allocated. This procedure requires knowledge of the segmentation result for the fundus image. In the segmented image, there are zones for which

exposure to laser light is forbidden. When solving the majority of problems of biomedical image recognition and diagnostics, textural features are used [64,103,104,125–129]. There are a large number of textural features. In this article, three groups of features are calculated, namely: (i) histogram features; (ii) gradient signs; and (iii) Haralik signs. The textural features are used to highlight blood vessels, exudates, and other details in the fundus image. In the general case, the textural features are statistical characteristics of a multidimensional probabilistic distribution of the brightness across a grayscale image. The work [126] considered a complete set of possible variants of features. Statistical signs of the second and third orders were discussed. These features were calculated from a halftone image. For color images, individual color channels were analyzed as grayscale images. In the simplest case, the features calculated for each channel were combined into one common set.

To calculate the informative feature space, the fundus images are first fragmented into certain regions of interest (ROI), which are characterized by the presence of various classes of objects, such as exudates, thick vessels, thin vessels, healthy areas, and others. At the initial stage, using a set of fundus images, the doctor-expert identifies the corresponding pathological and anatomical elements. The presence of such a sample makes it possible to analyze both individual classes and a set of selected classes.

Anatomical elements have a regular structure in the fundus image. The optic nerve head is always located on the left or right side of the fundus image, the favela is approximately in the center, the blood vessels are a tree-like structure outgoing from the optic nerve head, and the further the vessels branch, the thinner they appear. Among the pathological elements in the fundus image, standing out are edema, exudates, and newly formed blood vessels. Edema is often determined by the accumulation of exudation zones and is usually observed near blood vessels. Exudation zones indicate that the disease has been developing for quite a long time. In a healthy fundus, no pathological elements are observed. In order to carry out more accurate segmentation, in [69,70], we proposed a technology for generating a set of effective features based on the analysis of the textural properties of the indicated classes of images using discriminant analysis. Four main classes were considered, including thick blood vessels, newly formed vessels, zone without pathologies and exudates. At the stage of image fragmentation, the image was divided into square blocks of a given size. Each block belonged to one of the four selected classes.

The works [72,76] proposed and studied technologies that are based on clustering methods and data mining using textural features. An analysis of ROI of the original images showed them to have essentially different textural properties. For research purposes, initial samples of sliced images were formed from the original ones in various combinations of color space components. The well-known MaZda library [130] was used to calculate textural features from the sliced images. The calculated features were subjected to intellectual analysis using the proposed technologies. For example, in [64], we showed that the best results were obtained when using the Mahalanobis measure and features selected using a pairwise selection technique. Modifications of the technology were also proposed in [71,72], which has made it possible to improve accuracy when using morphological operations.

The proposed technologies for the intellectual analysis of textural features that focus on the analysis of arbitrary textural features [104], including their selection, were tested on real images of the fundus. Furthermore, in [69], it was shown that the preferred number of features is 6, and the optimal size of the segmentation window is 12. The most informative color channel is green and color channels of the HSV-format were also found to be informative. Figure 2 shows an example of the fundus image segmentation, with four main classes identified, including thick blood vessels, thin vessels, exudates, and the background.

Figure 2. An example of segmentation of the fundus image.

In [131], segmentation was performed based on the classification of texture features calculated from the neighborhoods of pixels using decision trees.

Decision trees make it possible not only to classify data but also to identify informative features. An analysis of the decision trees showed that most of the trees separate the "vessels" class from the "background" class by the SumAverage feature in the green or blue channel of the fundus image. The "thin vessels" class is best separated from the "thick vessels" class by the Skewness sign in the green channel of the image.

The segmentation based on texture features has a key drawback, which is high computational complexity. Because of this, different approaches have been proposed. In the publication [132], we developed a high-performance algorithm for calculating texture features, which has made it possible to speed up calculations by approximately an order of magnitude. Approaches related to the use of neural networks were also used [73,108,133]. Neural networks have made it possible to provide segmentation of the fundus image in a fairly short period of time. At the same time, the accuracy was found to be sufficient to use the segmentation result in the laser coagulation support system.

The segmentation results allow us to highlight selected zones prohibited from the coagulation, such as blood vessels, an optic nerve head, and other elements. At the same time, coagulation has a strong side-effect causing the retinal inflammation, so only pathological retinal areas should be exposed to laser light. Macular edema that undergoes coagulation is found in an area where the retina is normally enlarged. The zone of laser exposure is highlighted based on identifying the thickness of the retina and zones with anatomical and pathological features [134].

3.2. Algorithms for Generating a Preliminary Coagulation Plan in the Area of Laser Exposure

Automatic formation of a preliminary coagulation plan in the laser exposure zone includes a stage of identifying potential centers of circles and a stage of arranging centers with a specified minimum distance.

Characteristics of a point laser impact depend on the location of the target point. For example, the power and duration of the pulse should be calculated based on the structure of the retina at a given point [35]. The main task of forming a preliminary coagulation plan in the area of laser exposure is that of placing centers of the circles in such a way that the circles are inside the specified area, do not overlap, cover the area of laser exposure as densely as possible and meet the specified criteria [74,75]. The laser spot radius is 100 μm. The affected area of coagulation is no larger than the spot area and is generally independent of the laser parameters. Thus, all circles have the same radius. The safe distance between centers of the coagulates was estimated in [54] and found to be approximately 180 μm.

As input data, a binary image with a selected area of laser exposure is considered [74]. Accordingly, the result of the algorithm execution is discrete points in the image. The problem of arranging circles is easily reduced to a problem of placing points in a certain area that satisfy given criteria, if we search for potential centers of circles. The potential center of the circle is a point in the area of laser exposure around which it is possible to form

a circular neighborhood of a given radius, which is included in the area of laser exposure. Let us designate the area of laser impact as Q. The binary image is defined by the formula:

$$f_{ij} = \begin{cases} 1, (i,j) \in Q \\ 0, (i,j) \notin Q \end{cases} \quad (1)$$

Considering the above-said, point (i_0, j_0) is the potential center of the circle if condition (2) is 'True'.

$$\forall (i,j) \in B_r(i_0, j_0) : f_{ij} = 1, \quad (2)$$

where $B_r(i,j)$ is a circle with the center coordinates (i,j) and radius r. After calculating all the potential centers of circles, a new region is formed any point of which satisfies one of the safety conditions, i.e., the laser cannot enter the prohibited regions. Figure 3 shows the selected zone of laser exposure, transformed into the area of potential centers of circles (Figure 3a).

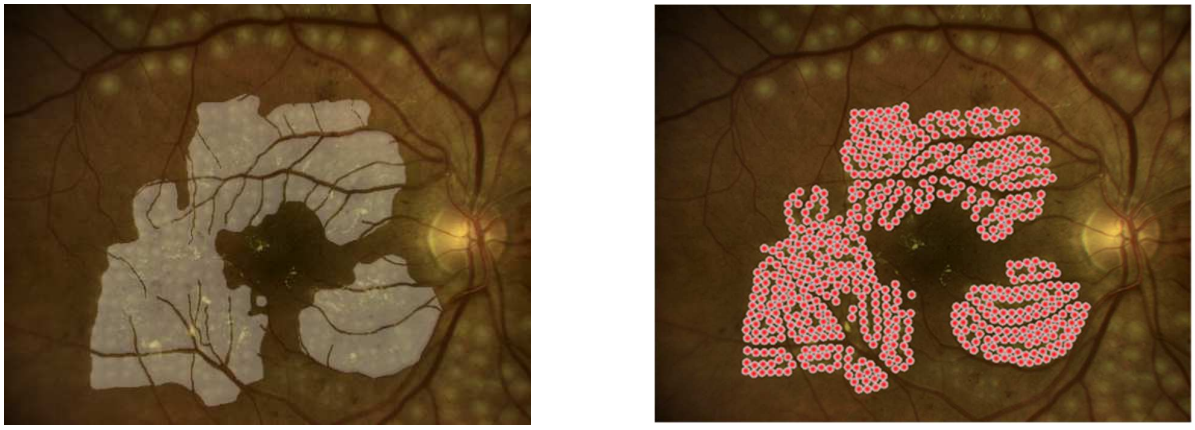

(**a**) (**b**)

Figure 3. (**a**) An image with a selected area of potential centers of circles, obtained from the area of laser exposure; (**b**) the result of filling the zone with coagulates.

After that, the centers of coagulates are located in the obtained area. Then, the result of the placement of coagulates is consistent with the original image and superimposed on the fundus image (Figure 3b). To check condition (1) at some point, it is necessary to go around all the points belonging to the circle centered at the point under consideration.

For a simple mathematical notation of the algorithm, we introduce the concept of a circular mask:

$$m_{ij} = \begin{cases} 1, i^2 + j^2 \leq r^2 \\ 0, i^2 + j^2 > r^2 \end{cases}, -r \leq i, j \leq r \quad (3)$$

Mask sizes are $(2r+1) \times (2r+1)$. If the point (i,j) is checked for condition (2), it is necessary to consider all points $-r \leq k,\ l \leq r$, which correspond to the values (3), determined by the mask, and $f_{i+k\ j+l}$, determined by the original binary image. Given two binary values, a binary operation is performed that returns 'True' if the point passes the test. If all points pass the test, then the given point is the potential center of the circles. Table 1 shows possible values of the mask point and source image point, as well as the result that the binary operation should produce. The results given in the table correspond to the binary operation of implication; thus, a discrete version of condition (2) is written in the form $c_{ij} = \bigcap_{k=-r}^{r} \bigcap_{l=-r}^{r} \left[f_{i+k\ j+l} \to m_{kl} \right]$.

Table 1. The result of a binary operation between the value of the mask and the value of the original image.

m_{kl}	$f_{i+k\ j+l}$	Comment	Result
0	0	$(i+k, j+l) \notin B_r(i,j)$, so $f_{i+k\ j+l}$ can take any values	1
0	1		1
1	0	$(i+k, j+l) \in B_r(i,j)$, but the point is outside the zone Q	0
1	1	$(i+k, j+l) \in B_r(i,j)$, but the point is inside the zone Q	1

In this case, for each pixel of the original image, the number of operations is $4r^2 + 4r + 1$. When placing points in the laser impact zone, the minimum distance between the points is taken into account. The points are arranged in such a way that, according to a given pattern, the area is filled maximally densely.

In [83], nine algorithms for the coagulates plan formation were developed. Among them, regular algorithms based on the construction of a translation mesh given by the translation vectors $\overline{a}$ and $\overline{b}$ and described by the multitude $Y_{\phi\overline{s}}^{\overline{a}\overline{b}} = \left\{\overline{y} = \Phi_{\phi\overline{s}}\left[i\overline{a} + j\overline{b}\right] : i, j \in \mathbb{Z}, \overline{y} \in Q\right\}$, where Q is area of model, Q is laser impact zone, $\Phi_{\phi\ \overrightarrow{s}}[\overline{x}] = \mathrm{M}_\phi\overline{x} + \overline{s}$ is linear transformation, M_ϕ is the rotation matrix, $\overline{s}$ is the displacement vector, which is irregular, based on an iterative search for free potential centers and performing an operation of the form $C_{k+1} = C_k / B_r(\overline{x})$, where $B_r(\overline{x})$ is a set of points corresponding to a circle with radius r and center $\overline{x}$, and C_k is a set of free potential centers per iteration k. Regular algorithms select the rotation matrix and displacement vector in such a way that the maximum number of coagulates is in the laser impact zone. Square and hexagonal algorithms have been developed in which the angle between the translation vectors is 90° for a square map and 120° for a hexagonal one. Irregular maps are based on specifying a pattern along which iterations are carried out. Thus, a random map is based on a random selection of a free potential center. The wave map forms waves along which coagulates are filled. An ordered map chooses the first free potential center that comes across as a result of a left-to-right traversal. The boundary map defines the boundary and fills it with coagulates. The adaptive-boundary map is based on the same logic as the boundary map, but before filling the boundary, it selects the arrangement at which the maximum number of coagulates will fill the boundary. Algorithms were also proposed that combine regular maps with a boundary map [135]: the boundaries of local areas are distinguished, which are filled with regular maps [74].

For example, let us consider an algorithm based on wave filling of the given area with circles. The wave is such a sequence of points $G = (\overline{g}_i)_{i=\overline{1,K}}$ that is constructed according to the following iterative process: $\overline{g}_{k+1} = \overline{g}_k + \overline{p}_k$, where $\overline{p}_k$ is a unit vector of the direction.

To formalize the algorithm for constructing a wave, we introduce the following notation: $\overline{e}_s$ is a unit vector in direction s, which takes a value from 1 to 4. The value 1 corresponds to the vector $\begin{pmatrix}0 & 1\end{pmatrix}$, with the remaining values corresponding to the clockwise rotation of this vector by 90°, 180° and 270°, respectively. $P^l = \left(\overline{e}_{(i+l-1) \bmod 4+1}\right)_{i=\overline{0,3}}$ is the base direction matrix with rotational offset l. The rotary displacement determines the priority direction, that is, the displacement characterizes the state of the wave at the current iteration, which tells in which direction the wave is moving at the current iteration. At each iteration, a matrix of basic directions is formed with the current rotational displacement l and then irrelevant directions are excluded from this matrix. The first such direction is the opposite of the current one. So, the wave should not change its direction to the opposite. This direction is the third column of the matrix of basic directions, because such a direction corresponds to 180° relative to the current direction (the first column of the matrix). Of the remaining three directions, it is necessary to exclude those that will lead to one of the points of the generated wave and to a point that does not belong to the laser impact zone.

The set of irrelevant directions due to the return to the current wave is described by the formula $T_P^k = \{\overline{p} = P : \overline{g}_k + \overline{p} \in G_k\}$. The set of irrelevant directions due to going beyond

the laser impact zone is described by the formula $R_P^k = \{\overline{p} = P : \overline{g}_k + \overline{p} \notin C_k\}$, where C_k is the area of potential circle centers at iteration k.

Let the matrix formed from the matrix of basic directions at iteration k be denoted as $\overline{P}_k$. It should be noted that this matrix excludes the third column corresponding to the opposite vector. Columns belonging to the set $T^k_{\overline{P}_k} \cup R^k_{\overline{P}_k}$ are excluded from the matrix $\overline{P}_k$. Thus, a matrix P_k is formed. In this case, if the first vector of the matrix is excluded, then the state l is modified so that l corresponds to the first vector of the given matrix after excluding irrelevant directions. If the matrix P_k is found to be empty (all four directions have been excluded), then the wave is considered to be built. If at least one column remains in the matrix, then the vector of the first column will correspond to the direction at the current iteration, so the state l must match it after matrix transformation. If the matrix P_k is zero filled, then the wave is considered to reach a dead end and assumed to be formed. The wave $G = (\overline{g}_i)_{i=\overline{1,K}}$ represents a curve on which it is necessary to place points, taking into account the criterion of the minimum distance between the points. Such an algorithm is written in the following iterative form: $X_t = X_{t-1} \cup \overline{g}_t; \overline{x}_t = \overline{g}_t, if\ |\overline{g}_t - \overline{x}_{t-1}| \geq 2r, t = \overline{2,K}$, where $\overline{x}_1 = \overline{g}_1$, $X_1 = \{\overline{x}_1\}$. Thus, the wave is transformed into a set of centers lying on the given wave. It should be noted that the algorithm for converting a wave into a set of centers is performed at each iteration of the algorithm. Let us denote the result of selecting the centers of circles on the current wave as X_k. In the last step, the circles are outside the area C_k. The centers of such circles correspond to the points of the set X_k. Then, at the next iteration, the area is expressed by the formula $C_{k+1} = C_k / \bigcup\limits_{\overline{x} \in X_k} B_r(\overline{x})$. The wave must have an initial approximation, namely a point from which the wave begins to travel. Such a point is determined using the algorithm $\overline{x} = next[C]$, which was presented in [74]. That is, we assume that at the iteration k, the expression $\overline{g}_1 = next[C_k]$ will provide a new point. Thus, the algorithm is an iterative process, where at each iteration a wave is formed, which is transformed into a set of circle centers, and a new area with excluded circles is created. The algorithm launches waves until the entire area is filled, that is, until the condition $C_k = \varnothing$ is fulfilled. The corresponding implementation of the algorithm is called a *wave map*. Figure 4 shows the performance of the algorithms for calculation the number of packed spheres. The lowest quality has the algorithm based on the use of the square grid. The best solution was for the algorithm based on adaptive boundary filling of spheres (adaptive boundary map).

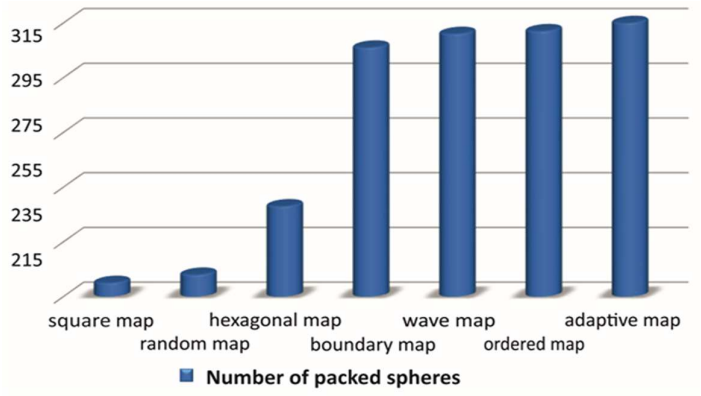

Figure 4. Comparative analysis of coagulate location algorithms.

An important problem is analyzing the mutual arrangement of coagulates as a result of planning. Characteristics of the coagulation plan are able to provide a prognosis of the laser coagulation outcome. In any case, to be able to estimate its various properties, the preliminary plan needs to be quantitatively described. We note that the preliminary plan can be mapped using an arbitrary technique, including a manual one. The coagulation plan comprises an array of points each of which is characterized by certain parameters. The parameters affect the degree of burn at the exposed points and can be evaluated using a technique described in [54,84].

The laser treatment parameters can be fitted In an optimal way at any layout of points given that the minimal distance is observed. With all the points known to be located in the ROI that needs to be exposed to laser treatment, inter-point distances come to the forefront. For a distance sampling to be generated, a point-connecting technique needs to be chosen based on a rule, for instance, by conducting a Delaunay triangulation relative to marked points (Figure 5). Next, using a standard Euclidean measure, values of the distances are calculated and written into a general sampling. Noise distances are then excluded and statistical characteristics are calculated, before being written in the general set of features (Table 2). Based on their expertise, ophthalmologists [35,136] suggest using statistical characteristics, such as the variance of mutual distances, the mathematical mean, and so on. Thus the effectiveness of a coagulation pattern can be estimated by calculating a number of features relating to the mutual position of coagulates. As far as a minimal inter-coagulate distance is observed, mapping a coagulation pattern within a pathological zone guarantees safe coagulation because such an approach enables one to exclude two possible problems. The first is exposure of prohibited areas to the laser light, and the second is excessive retina damage due to a very small distance between neighboring coagulates.

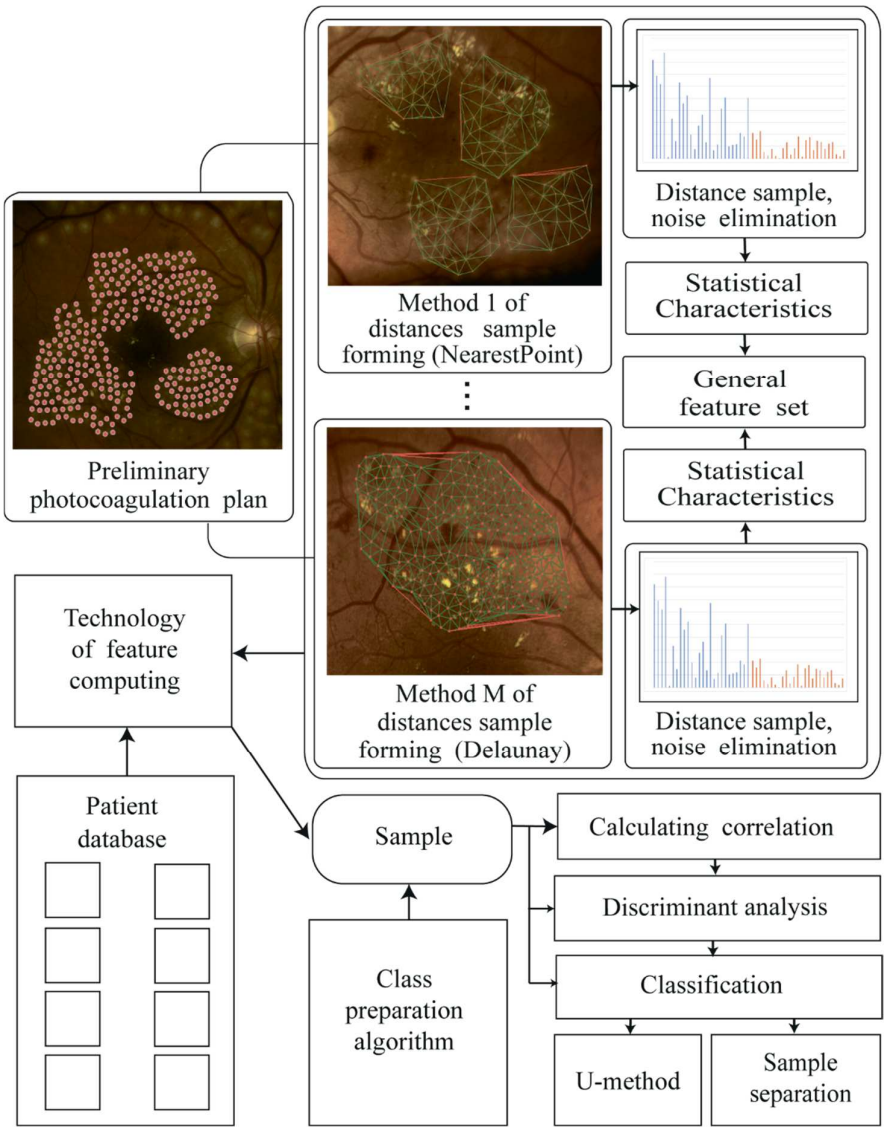

Figure 5. Scheme of the intelligent analysis of the photocoagulation plan.

Table 2. Feature values for various algorithms for mapping a coagulation plan.

Algorithm	Variance	Median	Number
Random map	6.32	31.62	223
Square map	6.09	30.00	220
Hexagonal map	7.68	30.00	248
Wave map	0.95	30.08	311
Boundary map	0.90	30.08	305
Boundary-adaptive map	0.70	30.07	315
Ordered map	0.19	30.08	312

Medical doctors used to analyze the uniformity of the coagulation pattern primarily based on the variance. The features used include various statistical characteristics of the inter-coagulate distance (a mutual location feature) and features corresponding to the coagulation pattern volume and the area covered (general features) [74].

These characteristics form a basis for evaluating the uniformity and balance of the coagulation pattern. Alongside statistical characteristics, an important feature is the number of laser impact points in the coagulation plan. As an extra feature, the number of local regions in the coagulation pattern may be used. In total, 26 features were selected and then analyzed using an in-house technology of intelligent data analysis (Figure 5).

The technology allows for analyzing the classification quality of both initial features and features selected based on discriminant analysis, which relies on evaluating the linear separability of classes. Discriminant analysis aims to transform the initial features so as to maximize the separability criterion.

The proposed techniques have formed a basis for a technology of mapping a photocoagulation pattern, allowing the efficacy of DR treatment to be enhanced (Figure 1).

Figure 6 shows an example of applying the method of automatic formation of a coagulation plan in the fundus image. Certain areas are highlighted in different colors, to mark areas forbidden from the laser impact, whereas the automatically generated pattern of laser coagulation is marked by circles.

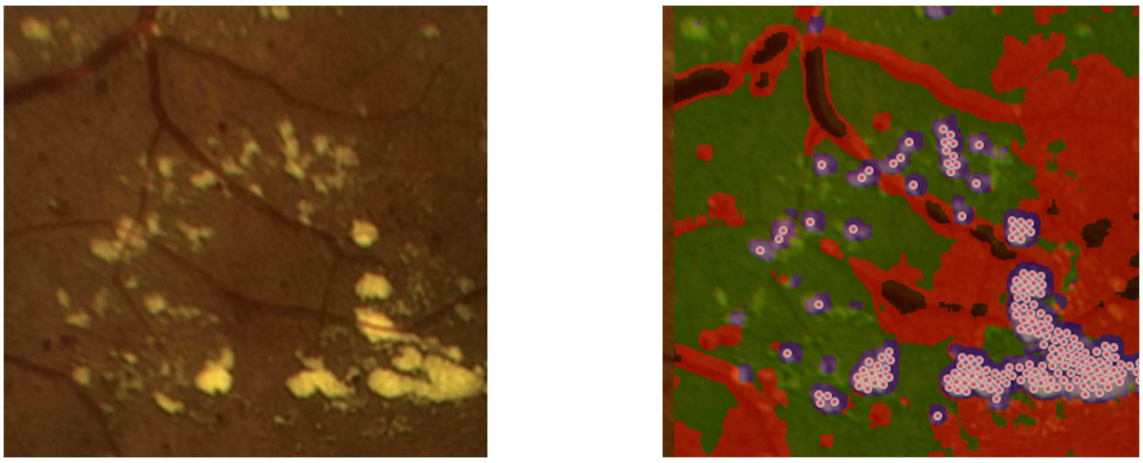

(**a**) (**b**)

Figure 6. Results of filling the selected ROI with coagulates: (**a**) zone of exudate; (**b**) the result of filling with coagulates.

Such images can also be effectively processed by detection algorithms [137]. The ophthalmologist will be able to correct the processing result for any block in the diagram in Figure 1. For instance, the ophthalmological surgeon may correct the outline of the ROIs for laser treatment if in their opinion the ROIs have not all been automatically marked off.

The methods of fundus image segmentation and coagulation placement described above represent the key steps for the formation of a coagulation plan since it is these

steps that provide significant support in the manual formation of the coagulation plan. Among the presented stages (Figure 1), the first stage of data combination is a manual algorithm for placing key points. For doctors, the placement of key points is not difficult. The problem lies precisely in the manual arrangement of coagulates since in the manual mode this is a very laborious process. For the pathological zone to be isolated, information is needed on deviations of the retinal thickness from the norm. This information is provided by the medical SOCT software. The result produced by the software implementation is pre-processed, and a map of retinal deviations from the norm is formed. An excessive deviation is a sign of pathology in this area.

A reconstructed fundus image from OCT images is required to match this image with the fundus image obtained from the fundus camera. This image is also generated using the SOCT software. The proposed system assumes that the doctor places key points in the reconstructed image and in the fundus image. Afterwards, the pathological zone is highlighted, which is combined with the image of the fundus. The zone of laser exposure is formed on the basis of the result of segmentation of forbidden areas, the selected pathological zone and the result of manual correction by an ophthalmologist.

At the final step, a coagulation plan is formed, for which its quality characteristics are calculated, and the success of laser coagulation is also assessed. The described method of forming a coagulation plan corresponds to a new method for the treatment of DR [35] and demonstrates an increase in the effectiveness of treatment compared to the navigation method [41]. The above-described technology has formed the basis of a computerized system for mapping and analyzing a preliminary coagulation pattern for DR laser treatment. Figure 7 shows a graphic interface of the system.

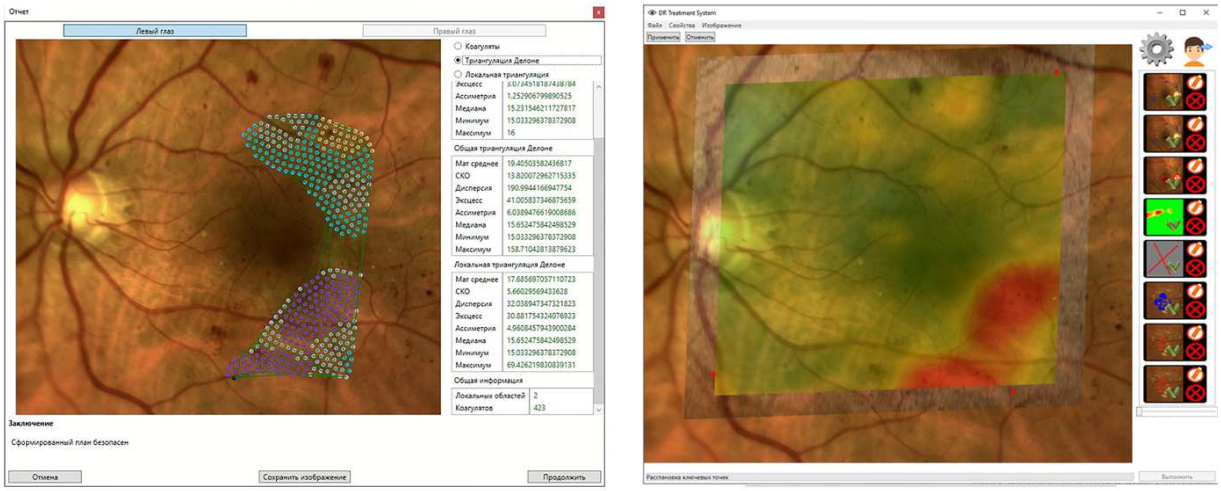

Figure 7. An example of the operation of the photocoagulation plan formation system.

Functionality of the system is as follows: manual placement of key points on the OCT image and the fundus image; visualization of the intermediate processing steps by the software package; setting up data processing stages; visualization of the final coagulation plan indicating the assessment of photocoagulation signs.

In the future, the optimization of intellectual image processing algorithms [138,139] are planned.

4. Conclusions

The article has presented the development of a computer system for automatically generating a laser coagulation plan to improve the quality of retinal coagulation in the treatment of DR. An overview of the main methods and algorithms that have formed the basis of the coagulation plan planning system is presented.

An analysis of existing laser coagulation methods in the treatment of diabetic retinopathy has shown that modern treatment methods do not provide the required efficacy of retinal laser coagulation treatment, as the laser energy is nonuniformly distributed across the pigment epithelium and may exert an excessive effect on parts of the retina and anatomical elements. The overview results have shown that the effectiveness of retinal laser coagulation for the treatment of DR is determined by the relative position of coagulates and parameters of laser exposure. The following stages of processing diagnostic data for the formation and intellectual analysis of a preliminary coagulation plan have been identified: selection of the laser exposure zone, evaluation of safe parameters of the laser pulse to the fundus, formation of a coagulation plan in the laser exposure zone, and analysis of the generated plan to predict the therapeutic effect.

A methodological and algorithmic software called "DR Treatment System" has been developed. The software allows ophthalmologists to automatically generate preliminary coagulation plans for the effective treatment of DR with the possibility of correcting the main stages of treatment, adding to the functionality of the modern NAVILAS system, which includes automatic laser guidance according to the generated plan, while not providing automatic formation of a preliminary coagulation plan. The software provides the ability to evaluate the main characteristics of a preliminary coagulation plan, predict the therapeutic effect of retinal laser coagulation, and form a recommended treatment plan for DR, which can increase the safety and efficiency of the operation.

Summing up, in writing the article, we set ourselves a goal of providing ophthalmic surgeons with an intelligent system that would offer a recommended treatment plan using individual patient data in a matter of a few seconds just prior to the surgical procedure. The smart system discussed in this paper will allow doctors to monitor the recommended treatment plan for diabetic retinopathy in a real time mode. At the final stage of research, we also plan to equip the technology with an augmented reality system. Then, ophthalmic surgeons will obtain an instrument for checking the ongoing surgical procedure in real time against the operation plan recommended by the developed smart system.

The study was approved by Bioethics Commission for Research at Samara State Medical University. The digital images used in this study were acquired with all the required authorizations. Furthermore, each patient signed a form to provide consent for this study and each acquired image has been treated anonymously. All of the experiments presented were carried out in accordance with the approved guidelines.

Author Contributions: Methodology, N.D. and N.I.; validation, N.D. and N.A.; writing—original draft, N.I. and N.D.; writing—review and editing, N.A.; supervision, N.I.; funding acquisition, N.I. This article is based on the thesis of the 14th KES-IDT 2022 Conference "Automated System for the Personalization of Retinal Laser Treatment in Diabetic Retinopathy Based on the Intelligent Analysis of OCT Data and Fundus Images" by Nataly Ilyasova, Nikita Demin, Alexandr Shirokanev and Nikita Andriyanov. However, this article considers an absolutely new review and description of methods used for laser coagulation and describes computer system functionality in detail. All authors have read and agreed to the published version of the manuscript.

Funding: The Russian Foundation for Basic Research (19-29-01135) and the Ministry of Science and Higher Education of the Russian Federation within (Government project).

Institutional Review Board Statement: Not applicable.

Informed Consent Statement: Not applicable.

Data Availability Statement: Data is unavailable due to privacy and ethical restrictions.

Acknowledgments: This work was partly funded by the Russian Foundation for Basic Research and the RF Ministry of Science and Higher Education under a government project of FSRC "Crystallography and Photonics" RAS and Samara University.

Conflicts of Interest: The authors declare no conflict of interest.

References

1. Rottier, J.B. Artificial intelligence: Reinforcing the place of humans in our healthcare system. *Rev. Prat.* **2018**, *68*, 1150–1151. [PubMed]
2. Fourcade, A.; Khonsari, R.H. Deep Learning in Medical Image Analysis: A third eye for doctors. *J. Stomatol. Oral Maxillofac. Surg.* **2019**, *120*, 279–288. [CrossRef]
3. Bodapati, J.D.; Naralasetti, V.; Shareef, S.N.; Hakak, S.; Bilal, M.; Maddikunta, P.K.; Jo, O. Blended multi-modal deep convnet features for diabetic retinopathy severity prediction. *Electronics* **2020**, *9*, 914. [CrossRef]
4. Budai, A.; Bock, R.; Maier, A.; Hornegger, J.; Michelson, G. Robust vessel segmentation in fundus images. *Int. J. Biomed. Imaging* **2013**, *2013*, 154860. [CrossRef] [PubMed]
5. Kermany, D.S.; Goldbaum, M.; Cai, W.; Valentim, C.C.S.; Liang, H.; Baxter, S.L.; McKeown, A.; Yang, G.; Wu, X.; Yan, F.; et al. Identifying medical diagnoses and treatable diseases by image-based Deep Learning. *Cell* **2018**, *172*, 1122–1131. [CrossRef]
6. Ojie, O.D.; Saatchi, R. Kohonen Neural Network Investigation of the Effects of the Visual, Proprioceptive and Vestibular Systems to Balance in Young Healthy Adult Subjects. *Healthcare* **2021**, *9*, 1219. [CrossRef]
7. Ahsan, M.M.; Nazim, R.; Siddique, Z.; Huebner, P. Detection of COVID-19 Patients from CT Scan and Chest X-ray Data Using Modified MobileNetV2 and LIME. *Healthcare* **2021**, *9*, 1099. [CrossRef]
8. Eckstein, J.; Moghadasi, N.; Körperich, H.; Weise Valdés, E.; Sciacca, V.; Paluszkiewicz, L.; Burchert, W.; Piran, M. A Machine Learning Challenge: Detection of Cardiac Amyloidosis Based on Bi-Atrial and Right Ventricular Strain and Cardiac Function. *Diagnostics* **2022**, *12*, 2693. [CrossRef]
9. Lee, J.H.; Lee, J.; Cho, S.; Song, J.E.; Lee, M.; Kim, S.H.; Lee, J.Y.; Shin, D.H.; Kim, J.M.; Bae, J.H.; et al. Development of Decision Support Software for deep learning-based automated retinal disease screening using relatively limited fundus photograph data. *Electronics* **2021**, *10*, 163. [CrossRef]
10. Ghani, A.; See, C.; Sudhakaran, V.; Ahmad, J.; Abd-Alhameed, R. Accelerating retinal fundus image classification using artificial neural networks (Anns) and reconfigurable hardware (FPGA). *Electronics* **2019**, *8*, 1522. [CrossRef]
11. Gao, A.; Murphy, R.R.; Chen, W.; Dagnino, G.; Fischer, P.; Gutierrez, M.G.; Kundrat, D.; Nelson, B.J.; Shamsudhin, N.; Su, H.; et al. Progress in robotics for Combating Infectious Diseases. *Sci. Robot.* **2021**, *6*, 1–17. [CrossRef]
12. Strzelecki, M.; Szczypinski, P.; Materka, A.; Klepaczko, A. A software tool for automatic classification and segmentation of 2D/3D Medical Images. *Nucl. Instrum. Methods Phys. Res. A Accel. Spectrom. Detect. Assoc. Equip.* **2013**, *702*, 137–140. [CrossRef]
13. Jamil, M.F.; Pokharel, M.; Park, K. Light-Controlled Microbots in Biomedical Application: A Review. *Appl. Sci.* **2022**, *12*, 1013. [CrossRef]
14. Trinh, M.; Ghassibi, M.; Lieberman, R. Artificial Intelligence in retina. *Adv. Ophthalmol. Optom.* **2021**, *6*, 175–185. [CrossRef]
15. Luo, L.; Xue, D.; Feng, X. Automatic Diabetic Retinopathy Grading via Self-Knowledge Distillation. *Electronics* **2020**, *9*, 1337. [CrossRef]
16. Wang, R.; Miao, Z.; Liu, T.; Liu, M.; Grdinovac, K.; Song, X.; Liang, Y.; Delen, D.; Paiva, W. Derivation and Validation of Essential Predictors and Risk Index for Early Detection of Diabetic Retinopathy Using Electronic Health Records. *J. Clin. Med.* **2021**, *10*, 1473. [CrossRef]
17. Vorobieva, I.V.; Merkushenkova, D.A. Diabetic retinopathy in patients with type 2 Diabetes Mellitus. Epidemiology, a modern view of pathogenesis. *Ophthalmology* **2012**, *9*, 18–21.
18. Elgafi, M.; Sharafeldeen, A.; Elnakib, A.; Elgarayhi, A.; Alghamdi, N.S.; Sallah, M.; El-Baz, A. Detection of Diabetic Retinopathy Using Extracted 3D Features from OCT Images. *Sensors* **2022**, *22*, 7833. [CrossRef]
19. Ansari, P.; Tabasumma, N.; Snigdha, N.N.; Siam, N.H.; Panduru, R.V.N.R.S.; Azam, S.; Hannan, J.M.A.; Abdel-Wahab, Y.H.A. Diabetic Retinopathy: An Overview on Mechanisms, Pathophysiology and Pharmacotherapy. *Diabetology* **2022**, *3*, 11. [CrossRef]
20. Guariguata, L.; Whiting, D.R.; Hambleton, I.; Beagley, J.; Linnenkamp, U.; Shaw, J.E. Global estimates of diabetes prevalence for 2013 and projections for 2035. *Diabetes Res. Clin. Pract.* **2014**, *103*, 137–149. [CrossRef]
21. Tan, G.S.; Cheung, N.; Simo, R. Diabetic macular edema. *Lancet Diab. Endoc.* **2017**, *5*, 143–155. [CrossRef] [PubMed]
22. Amjad, R.; Lee, C.-A.; Farooqi, H.M.U.; Khan, H.; Paeng, D.-G. Choroidal Thickness in Different Patterns of Diabetic Macular Edema. *J. Clin. Med.* **2022**, *11*, 6169. [CrossRef] [PubMed]
23. Bratko, G.V.; Chernykh, V.V.; Sazonova, O.V. On early diagnostics and the occurence rate of diabetic macular edema and identification of diabetes risk groups. *Sib. Sci. Med. J.* **2015**, *35*, 33–36.
24. Klein, R.; Klein, B.E.K.; Moss, S.E.; Davis, M.D.; DeMets, D.L. The Wisconsin Epidemiologic Study of Diabetic Retinopathy IV. Diabetic Macular Edema. *Ophthalmology* **1984**, *91*, 1464–1474. [CrossRef] [PubMed]
25. Ixcamey, M.; Palma, C. Diabetic macular edema. *Dis.-A-Mon.* **2021**, *67*, 101138. [CrossRef]
26. Amirov, A.N.; Abdulaeva, E.A.; Minkhuzina, E.L. Diabetic macular edema: Epidemiology, pathogenesis, diagnosis, clinical presentation, and treatment. *Kazan Med. J.* **2015**, *96*, 70–74. [CrossRef]
27. Hamad, H.; Dwickat, T.; Tegolo, D.; Valenti, C. Exudates as Landmarks Identified through FCM Clustering in Retinal Images. *Appl. Sci.* **2021**, *11*, 142. [CrossRef]
28. Kozak, I.; Luttrull, J.K. Modern retinal laser therapy. *Saudi J. Ophthalmol.* **2015**, *29*, 137–146. [CrossRef]
29. Frizziero, L.; Calciati, A.; Torresin, T.; Midena, G.; Parrozzani, R.; Pilotto, E.; Midena, E. Diabetic Macular Edema Treated with 577-nm Subthreshold Micropulse Laser: A Real-Life, Long-Term Study. *J. Pers. Med.* **2021**, *11*, 405. [CrossRef]
30. Kotsur, T.V.; Izmailov, A.S. The effectiveness of laser coagulation in the macula and high-density microphotocoagulation in the treatment of diabetic maбculopathy. *Ophthalmol. Statements* **2016**, *9*, 43–45.

31. Artemov, S.; Belyaev, A.; Bushukina, O.; Khrushchalina, S.; Kostin, S.; Lyapin, A.; Ryabochkina, P.; Taratynova, A. Endovenous laser coagulation using two-micron laser radiation: Mathematical modeling and in vivo experiments. In Proceedings of the International Conference on Advanced Laser Technologies (ALT), Prague, Czech Republic, 15–20 September 2019; pp. 14–21.
32. Bianco, L.; Gawęcki, M.; Antropoli, A.; Arrigo, A.; Bandello, F.; Battaglia Parodi, M. Laser Treatment for Retinal Arterial Macroaneurysm. *Photonics* **2022**, *9*, 851. [CrossRef]
33. Xie, X.; Liu, Q.; Paulus, Y.M. Optical Coherence Tomography Following Panretinal Photocoagulation Demonstrating Choroidal Detachment. *Photonics* **2022**, *9*, 730. [CrossRef]
34. Zhang, J.; Zhang, J.; Zhang, C.; Zhang, J.; Gu, L.; Luo, D.; Qiu, Q. Diabetic Macular Edema: Current Understanding, Molecular Mechanisms and Therapeutic Implications. *Cells* **2022**, *11*, 3362. [CrossRef]
35. Zamytsky, E.A.; Zolotarev, A.V.; Karlova, E.V.; Zamytsky, P.A. Analysis of the coagulates intensity in laser treatment of diabetic macular edema in a Navilas robotic laser system. *Saratov J. Med. Sci. Res.* **2017**, *13*, 375–378.
36. Grzybowski, A.; Markeviciute, A.; Zemaitiene, R. Treatment of Macular Edema in Vascular Retinal Diseases: A 2021 Update. *J. Clin. Med.* **2021**, *10*, 5300. [CrossRef]
37. Gafurov, S.D.; Katakhonov, S.M.; Holmonov, M.M. Features of the use of lasers in medicine. *Eur. Sci.* **2019**, *3*, 92–95.
38. Da Pozzo, S.; Iacono, P.; Arrigo, A.; Battaglia Parodi, M. The Role of Imaging in Planning Treatment for Central Serous Chorioretinopathy. *Pharmaceuticals* **2021**, *14*, 105. [CrossRef]
39. Moutray, T.; Evans, J.R.; Lois, N.; Armstrong, D.J.; Peto, T.; Azuara-Blanco, A. Different lasers and techniques for proliferative diabetic retinopathy. *Cochrane Database Syst. Rev.* **2018**, *3(CD012314)*, 1–87. [CrossRef]
40. Frizziero, L.; Calciati, A.; Midena, G.; Torresin, T.; Parrozzani, R.; Pilotto, E.; Midena, E. Subthreshold Micropulse Laser Modulates Retinal Neuroinflammatory Biomarkers in Diabetic Macular Edema. *J. Clin. Med.* **2021**, *10*, 3134. [CrossRef]
41. Jung, J.J.; Gallego-Pinazo1, R.; Lleó-Pérez, A.; Huz, J.I.; Barbazetto, I.A. Navilas laser system focal laser treatment for diabetic macular edema—One-year results of a case series. *Open Ophthalmol. J.* **2013**, *7*, 48–53. [CrossRef]
42. Toto, L.; D'Aloisio, R.; Quarta, A.; Libertini, D.; D'Onofrio, G.; De Nicola, C.; Romano, A.; Mastropasqua, R. Intravitreal Dexamethasone Implant (IDI) Alone and Combined with Navigated 577 nm Subthreshold Micropulse Laser (SML) for Diabetic Macular Oedema. *J. Clin. Med.* **2022**, *11*, 5200. [CrossRef] [PubMed]
43. Chauhan, M.Z.; Rather, P.A.; Samarah, S.M.; Elhusseiny, A.M.; Sallam, A.B. Current and Novel Therapeutic Approaches for Treatment of Diabetic Macular Edema. *Cells* **2022**, *11*, 1950. [CrossRef] [PubMed]
44. Velichko, P.B. Comprehensive treatment of diabetic macular edema. *Bull. Russ. Univ. Math.* **2014**, *19*, 1097–1101.
45. Al Zabadi, H.; Taha, I.; Zagha, R. Clinical and Molecular Characteristics of Diabetic Retinopathy and Its Severity Complications among Diabetic Patients: A Multicenter Cross-Sectional Study. *J. Clin. Med.* **2022**, *11*, 3945. [CrossRef] [PubMed]
46. Tomita, Y.; Lee, D.; Tsubota, K.; Negishi, K.; Kurihara, T. Updates on the Current Treatments for Diabetic Retinopathy and Possibility of Future Oral Therapy. *J. Clin. Med.* **2021**, *10*, 4666. [CrossRef]
47. Goidin, A.P.; Fabrikantov, O.L.; Sukhorukova, E.V. The effectiveness of classical and pattern laser coagulation in diabetic retinopathy. Bulletin of Russian Universities. *Mathematics* **2014**, *19*, 1105–1107.
48. Zavgorodnya, N.G.; Bezugly, M.B.; Bezugly, B.S.; Sarzhevskaya, L.E. The use of lasers in ophthalmology: A manual for interns in the specialty "Ophthalmology". *Zaporozhye ZSMU* **2015**.
49. Miura, Y.; Inagaki, K.; Hutfilz, A.; Seifert, E.; Schmarbeck, B.; Murakami, A.; Ohkoshi, K.; Brinkmann, R. Temperature Increase and Damage Extent at Retinal Pigment Epithelium Compared between Continuous Wave and Micropulse Laser Application. *Life* **2022**, *12*, 1313. [CrossRef]
50. Danielescu, C.; Moraru, A.D.; Anton, N.; Bilha, M.-I.; Donica, V.-C.; Darabus, D.-M.; Munteanu, M.; Stefanescu-Dima, A.S. The Learning Curve of Surgery of Diabetic Tractional Retinal Detachment—A Retrospective, Comparative Study. *Medicina* **2023**, *59*, 73. [CrossRef]
51. Lipatov, D.V.; Smirnova, N.B.; Aleksandrova, V.K. Modern algorithm for laser coagulation of the retina in diabetic retinopathy. *Diabetes Mellit.* **2007**, *10*, 45–46. [CrossRef]
52. Dong, J.; Li, Q.; Wang, X.; Fan, Y. A Review of the Methods of Non-Invasive Assessment of Intracranial Pressure through Ocular Measurement. *Bioengineering* **2022**, *9*, 304. [CrossRef]
53. Abbas, S.M.; Rajaei, M.J.; Abrishami, M. Temperature Distribution Simulation of the Human Eye Exposed to Laser Radiation. *J. Lasers Med. Sci.* **2013**, *4*, 175–181.
54. Shirokanev, A.; Ilyasova, N.; Andriyanov, N.; Zamytskiy, E.; Zolotarev, A.; Kirsh, D. Modeling of Fundus Laser Exposure for estimating safe laser coagulation parameters in the treatment of diabetic retinopathy. *Mathematics* **2021**, *9*, 967. [CrossRef]
55. Sabal, B.; Teper, S.; Wylęgała, E. Subthreshold Micropulse Laser for Diabetic Macular Edema: A Review. *J. Clin. Med.* **2023**, *12*, 274. [CrossRef]
56. Silviya, S.; Anitha, C.M.; Prakash, P.S.G.; Bahammam, S.A.; Bahammam, M.A.; Almarghlani, A.; Assaggaf, M.; Kamil, M.A.; Subramanian, S.; Balaji, T.M.; et al. The Efficacy of Low-Level Laser Therapy Combined with Single Flap Periodontal Surgery in the Management of Intrabony Periodontal Defects: A Randomized Controlled Trial. *Healthcare* **2022**, *10*, 1301. [CrossRef]
57. Guo, S.; Wang, K.; Kang, H.; Liu, T.; Gao, Y.; Li, T. Bin Loss for hard exudates segmentation in fundus images. *Neurocomputing* **2020**, *392*, 314–324. [CrossRef]
58. Fraz, M.M.; Jahangir, W.; Zahid, S.; Hamayun, M.M.; Barman, S.A. Multiscale segmentation of exudates in retinal images using contextual cues and ensemble classification. *Biomed. Signal Process. Control* **2017**, *35*, 50–62. [CrossRef]

59. Kusakunniran, W.; Wu, Q.; Ritthipravat, P.; Zhang, J. Hard exudates segmentation based on learned initial seeds and iterative graph cut. *Comput. Methods Programs Biomed.* **2018**, *158*, 173–183. [CrossRef]
60. Fiandono, I.; Firdausy, K. Median filtering for optic disc segmentation in retinal image. *Kinet. Game Technol. Inf. Syst. Comput. Netw. Comput. Electron. Control* **2018**, 73–80. [CrossRef]
61. Ramani, G.R.; Balasubramanian, L. Macula segmentation and fovea localization employing image processing and heuristic based clustering for automated retinal screening. *Comput. Methods Programs Biomed.* **2018**, *160*, 153–163.
62. Jeong, Y.; Hong, Y.-J.; Han, J.-H. Review of Machine Learning Applications Using Retinal Fundus Images. *Diagnostics* **2022**, *12*, 134. [CrossRef] [PubMed]
63. Ilyasova, N.; Paringer, R.; Kupriyanov, A.; Kirsh, D. Intelligent feature selection technique for segmentation of fundus images. In Proceedings of the 2017 Seventh International Conference on Innovative Computing Technology (INTECH), Luton, UK, 16–18 August 2017; pp. 138–143.
64. Gayathri, S.; Gopi, V.P.; Palanisamy, P. A lightweight CNN for diabetic retinopathy classification from fundus images. *Biomed. Signal Process. Control* **2020**, *62*, 102115.
65. Savelli, B.; Bria, A.; Molinara, M.; Marrocco, C.; Tortorella, F. A multi-context CNN ensemble for small lesion detection. *Artif. Intell. Med.* **2020**, *103*, 101749. [CrossRef] [PubMed]
66. Morales, S.; Colomer, A.; Mossi, J.M.; Amor, R.; Woldbye, D.; Klemp, K.; Larsen, M.; Naranjo, V. Retinal layer segmentation in rodent OCT images: Local intensity profiles & fully convolutional Neural Networks. *Comput. Methods Programs Biomed.* **2021**, *198*, 105788. [CrossRef] [PubMed]
67. He, Y.; Carass, A.; Liu, Y.; Jedynak, B.M.; Solomon, S.D.; Saidha, S.; Calabresi, P.A.; Prince, J.L. Structured layer surface segmentation for retina oct using fully convolutional regression networks. *Med. Image Anal.* **2021**, *68*, 101856. [CrossRef]
68. Ilyasova, N.; Paringer, R.; Kupriyanov, A. Regions of interest in a fundus image selection technique using the discriminative analysis methods. *Comput. Vis. Graph.* **2016**, 408–417.
69. Ilyasova, N.Y.; Shirokanev, A.S.; Kupriyanov, A.V.; Paringer, R.A. Technology of intellectual feature selection for a system of automatic formation of a coagulate plan on Retina. *Comput. Opt.* **2019**, *43*, 304–315. [CrossRef]
70. Ilyasova, N.Y.; Shirokanev, A.S.; Paringer, R.A.; Kupriyanov, A.V.; Zolotarev, A.V. A modified technique for smart textural feature selection to extract retinal regions of interest using image pre-processing. *J. Phys. Conf. Ser.* **2018**, *1096*, 012095. [CrossRef]
71. Ilyasova, N.; Paringer, R.; Shirokanev, A.; Kupriyanov, A.; Ushakova, N. A smart feature selection technique for object localization in ocular fundus images with the aid of color subspaces. *Procedia Eng.* **2017**, *201*, 736–745. [CrossRef]
72. Shirokanev, A.S.; Ilyasova, N.Y.; Demin, N.S. Analysis of convolutional neural network for Fundus Image segmentation. *J. Phys. Conf. Ser.* **2020**, *1438*, 012016. [CrossRef]
73. Shirokanev, A.; Kirsh, D.; Ilyasova, N.; Kupriyanov, A. Investigation of algorithms for coagulate arrangement in fundus images. *Comput. Opt.* **2018**, *42*, 712–721. [CrossRef]
74. Ilyasova, N.; Shirokanev, A.; Kirsh, D.; Paringer, R.; Kupriyanov, A.; Zamycky, E. Development of coagulate map formation algorithms to carry out treatment by laser coagulation. *Procedia Eng.* **2017**, *201*, 271–279. [CrossRef]
75. Ilyasova, N.; Shirokanev, A.; Paringer, R.; Kupriyanov, A. Biomedical data analysis based on Parallel Programming Technology Application for computation features' effectiveness. In Proceedings of the ICFSP 2019: 5th International Conference on Frontiers of Signal Processing, Marseille, France, 18–20 September 2019; pp. 67–71.
76. Raku, A.; Shirokanev, A.; Degtyarev, A.; Kibitkina, A.; Ilyasova, N.; Zolotarev, A. Study of thermal field of the retina of the human eye in the laser exposure zone during numerical simulation based on the solution of the heat equation in the layered region. In Proceedings of the 2020 International Conference on Information Technology and Nanotechnology (ITNT), Samara, Russia, 26–29 May 2020; pp. 1–12.
77. Shirokanev, A.; Degtyaryov, A.; Kibitkina, A.; Raku, A.; Ilyasova, N. Development of Information Technology for selection of effective strategy of diabetic retinopathy treatment. In Proceedings of the 2020 12th International Conference on Bioinformatics and Biomedical Technology, Xi'an, China, 22–24 May 2020; pp. 1–5.
78. Shirokanev, A.S.; Kibitkina, A.S.; Ilyasova, N.Y.; Degtyarev, A.A. Methods of mathematical modeling of fundus laser exposure for therapeutic effect evaluation. *Comput. Opt.* **2020**, *44*, 809–820. [CrossRef]
79. Yi, S.-L.; Yang, X.-L.; Wang, T.-W.; She, F.-R.; Xiong, X.; He, J.-F. Diabetic Retinopathy Diagnosis Based on RA-EfficientNet. *Appl. Sci.* **2021**, *11*, 1035. [CrossRef]
80. Kupriyanov, A.V.; Ilyasova, N.Y.; Ananin, M.A.; Malafeev, A.M.; Ustinov, A.V. Estimation of the geometric parameters of the optic disc region on the image of the fundus. *Comput. Opt.* **2005**, *28*, 136–139.
81. Kupriyanov, A.V.; Ilyasova, N.Y.; Khramov, A.G.; Malafeev, A.M.; Titova, O.A. Determination of the parameters of the vessel bed using a three-dimensional local fan-shaped transformation. *Comput. Opt.* **2004**, *25*, 154–157.
82. Ilyasova, N.Y.; Kupriyanov, A.V.; Ananin, M.A.; Gavrilova, N.A. Measurement of biomechanical characteristics of vessels for early diagnosis of vascular pathology of the fundus. *Comput. Opt.* **2005**, *27*, 165–169.
83. Ilyasova, N.; Shirokanev, A.; Kirsh, D.; Demin, N.; Zamytskiy, E.; Paringer, R.; Antonov, A. Identification of prognostic factors and predicting the therapeutic effect of laser photocoagulation for DME treatment. *Electronics* **2021**, *10*, 1420. [CrossRef]
84. Soifer, V.A.; Ilyasova, N.Y.; Kupriyanov, A.V.; Khramov, A.G.; Ananin, M.A. Methods of computer analysis of diagnostic images of the fundus. *Technol. Living Syst.* **2008**, *5*, 61–71.
85. Ilyasova, N. Methods for digital analysis of human vascular system. literature Review. *Comput. Opt.* **2013**, *37*, 511–535. [CrossRef]

86. Ahsan, S.; Basit, A.; Ahmed, K.; Ali, L.; Shaheen, F.; Ulhaque, M.; Fawwad, A. Diagnostic accuracy of direct ophthalmoscopy for detection of diabetic retinopathy using fundus photographs as a reference standard. *Diabetes Metab. Syndr. Clin. Res. Rev.* **2014**, *8*, 96–101. [CrossRef] [PubMed]
87. Helal, H.G.; Rashed, M.H.; Abdullah, O.A.; Salem, T.I.; Daifalla, A. MicroRNAs (−146a, −21 and −34A) are diagnostic and prognostic biomarkers for diabetic retinopathy. *Biomed. J.* **2021**, *44*, S242–S251. [CrossRef] [PubMed]
88. Hervella, Á.S.; Rouco, J.; Novo, J.; Penedo, M.G.; Ortega, M. Deep multi-instance heatmap regression for the detection of retinal vessel crossings and bifurcations in eye fundus images. *Comput. Methods Programs Biomed.* **2020**, *186*, 105201. [CrossRef] [PubMed]
89. Akram, M.U.; Akbar, S.; Hassan, T.; Khawaja, S.G.; Yasin, U.; Basit, I. Data on fundus images for vessels segmentation, detection of hypertensive retinopathy, diabetic retinopathy and papilledema. *Data Brief* **2020**, *29*, 105282. [CrossRef] [PubMed]
90. Tufail, A.; Rudisill, C.; Egan, C.; Kapetanakis, V.V.; Salas-Vega, S.; Owen, C.G.; Lee, A.; Louw, V.; Anderson, J.; Liew, G.; et al. Automated Diabetic Retinopathy Image Assessment Software. *Ophthalmology* **2017**, *124*, 343–351. [CrossRef]
91. Ayhan, M.S.; Kühlewein, L.; Aliyeva, G.; Inhoffen, W.; Ziemssen, F.; Berens, P. Expert-validated estimation of diagnostic uncertainty for deep neural networks in diabetic retinopathy detection. *Med. Image Anal.* **2020**, *64*, 101724. [CrossRef]
92. Li, T.; Gao, Y.; Wang, K.; Guo, S.; Liu, H.; Kang, H. Diagnostic assessment of deep learning algorithms for diabetic retinopathy screening. *Inf. Sci.* **2019**, *501*, 511–522. [CrossRef]
93. Nielsen, K.B.; Lautrup, M.L.; Andersen, J.K.H.; Savarimuthu, T.R.; Grauslund, J. Deep learning–based algorithms in screening of diabetic retinopathy: A systematic review of diagnostic performance. *Ophthalmol. Retin.* **2019**, *3*, 294–304. [CrossRef]
94. Shimada, Y.; Shibuya, M.; Shinoda, K. Transient Increase and Delay of Multifocal Electroretinograms Following Laser Photocoagulations for Diabetic Macular Edema. *J. Clin. Med.* **2021**, *10*, 357. [CrossRef]
95. Ilyasova, N. Estimating the geometric features of a 3D vascular structure. *Comput. Opt.* **2014**, *38*, 529–538. [CrossRef]
96. Ilyasova, N.Y.; Korepanov, A.O.; Chikulaev, P.M. A method for highlighting the central lines of blood vessels in diagnostic images. *Comput. Opt.* **2006**, *29*, 146–151.
97. Kupriyanov, A.V.; Ilyasova, N.Y.; Ananin, M.A. Evaluation of diagnostic parameters of blood vessels on images of the fundus in the region of the optic nerve head. *Comput. Opt.* **2006**, *29*, 141–146.
98. Branchevsky, S.L.; Gavrilova, N.A.; Ilyasova, N.Y.; Khramov, A.G. Digital analysis system for diagnosing vascular pathology of the fundus. *Bull. Ophthalmol.* **2003**, *5*, 37–40.
99. Iliasova, N.Y.; Ustinov, A.V.; Branchevsky, S.L.; Durasov, A.B. Methods for estimating geometric parameters of retinal vessels using diagnostic images of Fundus. *SPIE Proc.* **1998**, *3348*, 316–325.
100. Ananin, M.A.; Ilyasova, N.Y.; Kupriyanov, A.V. Estimating directions of optic disk blood vessels in retinal images. *Pattern Recognit. Image Anal.* **2007**, *17*, 523–526. [CrossRef]
101. Silverstein, E.; Freedman, S.; Zéhil, G.-P.; Jiramongkolchai, K.; El-Dairi, M. The macula in pediatric glaucoma: Quantifying the inner and outer layers via optical coherence tomography automatic segmentation. *J. Am. Assoc. Pediatr. Ophthalmol. Strabismus* **2016**, *20*, 332–336. [CrossRef]
102. Septiarini, A.; Harjoko, A.; Pulungan, R.; Ekantini, R. Automatic detection of peripapillary atrophy in retinal fundus images using statistical features. *Biomed. Signal Process. Control* **2018**, *45*, 151–159. [CrossRef]
103. Odstrcilik, J.; Kolar, R.; Tornow, R.-P.; Jan, J.; Budai, A.; Mayer, M.; Vodakova, M.; Laemmer, R.; Lamos, M.; Kuna, Z.; et al. Thickness related textural properties of retinal nerve fiber layer in color fundus images. *Comput. Med. Imaging Graph.* **2014**, *38*, 508–516. [CrossRef]
104. Claro, M.; Veras, R.; Santana, A.; Araújo, F.; Silva, R.; Almeida, J.; Leite, D. An hybrid feature space from texture information and transfer learning for glaucoma classification. *J. Vis. Commun. Image Represent.* **2019**, *64*, 102597. [CrossRef]
105. Andriyanov, N.A.; Dementiev, V.E.; Kargashin, Yu.D. Analysis of the impact of visual attacks on the characteristics of neural networks in image recognition. *Procedia Comput. Sci.* **2021**, *186*, 495–502. [CrossRef]
106. Andriyanov, N. Methods for Preventing Visual Attacks in Convolutional Neural Networks Based on Data Discard and Dimensionality Reduction. *Appl. Sci.* **2021**, *11*, 5235. [CrossRef]
107. Paringer, R.A.; Mukhin, A.V.; Ilyasova, N.Y.; Demin, N.S. Neural network application for semantic segmentation of Fundus. *Comput. Opt.* **2022**, *46*, 596–602. [CrossRef]
108. Doga, A.V.; Kachalina, G.F.; Pedanova, E.K.; Biryukov, D.A. Modern aspects of diagnosis and treatment of diabetic macular edema. *Ophthalmol. Diabetes* **2014**, *4*, 51–59.
109. Dedov, I.I.; Shestakova, M.V.; Galstyan, G.R. The prevalence of type 2 diabetes mellitus in the adult population of Russia (nation study). *Diabetes Mellit.* **2016**, *19*, 104–112. [CrossRef]
110. Astakhov, Yu.S.; Shadrichev, F.E.; Krasavina, M.I.; Grigorieva, N.N. Modern approaches to the treatment of diabetic macular edema. *Ophthalmol. Statements* **2009**, *4*, 59–69.
111. Kernt, M.; Cheuteu, R.; Liegl, R.G.; Seidensticker, F.; Cserhati, S.; Hirneiss, C.; Haritoglou, C.; Kampik, A.; Ulbig, M.; Neubauer, A.S. Navigated focal retinal laser therapy using the NAVILAS® system for diabetic macula edema. *Ophthalmologe* **2012**, *109*, 692–698. [CrossRef]
112. Brehmer, M.; Hasan, M. Neodynium/YAG-laser coagulation of urinary tract haemangiomas causing macroscopic haematuria, 5 to 10-years follow-up. *Eur. Urol. Suppl.* **2019**, *18*, e392. [CrossRef]
113. Xiang, H.; Chen, B.; Wu, W.J.; Zhang, Y.; Jia, H. An integral mps model of blood coagulation by laser irradiation: Application to the optimization of multi-pulse nd:YAG laser treatment of Port-Wine Stains. *Int. J. Heat Mass Transf.* **2017**, *114*, 1220–1233. [CrossRef]

114. Katoh, N.; Peyman, G.A. Effects of laser wavelengths on experimental retinal detachments and retinal vessels. *Jpn. J. Ophthalmol.* **1988**, *32*, 196–210.
115. Yun, Y.; Ma, D.; Yang, M. Human–computer interaction-based decision support system with applications in Data Mining. *Future Gener. Comput. Syst.* **2021**, *114*, 285–289. [CrossRef]
116. Vega, A.; García-Saiz, D.; Zorrilla, M.; Sánchez, P. Lavoisier: A DSL for increasing the level of abstraction of data selection and formatting in data mining. *J. Comput. Lang.* **2020**, *60*, 100987. [CrossRef]
117. Huang, J.; Ersoy, O.K.; Yan, X. Fault detection in dynamic plant-wide process by multi-block slow feature analysis and support vector data description. *ISA Trans.* **2019**, *85*, 119–128. [CrossRef]
118. Zhang, Y.; Zhang, Q.; Chen, Z.; Shang, J.; Wei, H. Feature assessment and ranking for classification with nonlinear sparse representation and approximate dependence analysis. *Decis. Support Syst.* **2019**, *122*, 113064. [CrossRef]
119. Ayyıldız, H.; Arslan Tuncer, S. Determination of the effect of red blood cell parameters in the discrimination of iron deficiency anemia and beta thalassemia via neighborhood component analysis feature selection-based machine learning. *Chemom. Intell. Lab. Syst.* **2020**, *196*, 103886. [CrossRef]
120. Gao, J.; Li, L. A robust geometric mean-based subspace discriminant analysis feature extraction approach for image set classification. *Optik* **2019**, *199*, 163368. [CrossRef]
121. Ilyasova, N.; Demin, N.; Shirokanev, A.; Andriyanov, N. Automated System for the Personalization of Retinal Laser Treatment in Diabetic Retinopathy Based on the Intelligent Analysis of OCT Data and Fundus Images. In *Intelligent Decision Technologies. Smart Innovation, Systems and Technologies*; Czarnowski, I., Howlett, R.J., Jain, L.C., Eds.; Springer: Berlin/Heidelberg, Germany, 2022; Volume 309, pp. 171–181.
122. Andriyanov, N.; Tashlinsky, A.; Dementiev, V. Detailed Clustering Based on Gaussian Mixture Models. In: Arai, K., Kapoor, S., Bhatia, R. (eds) Intelligent Systems and Applications. *Adv. Intell. Syst. Comput.* **2021**, *1251*, 437–448.
123. Deák, G.G.; Bolz, M.; Ritter, M.; Prager, S.; Benesch, T.; Schmidt-Erfurth, U. A systematic correlation between morphology and functional alterations in diabetic macular edema. *Investig. Opthalmol. Vis. Sci.* **2010**, *51*, 6710. [CrossRef]
124. Ilyasova, N.Y.; Kupriyanov, A.V.; Paringer, R.A. The discriminant analysis application to refine the diagnostic features of blood vessels images. *Opt. Mem. Neural Netw.* **2015**, *24*, 309–313. [CrossRef]
125. Ilyasova, N.Y.; Kupriyanov, A.V.; Khramov, A.G. Information technologies of image analysis in the problems of medical diagnostics. *Radio Commun.* **2012**.
126. Daginawala, N.; Li, B.; Buch, K.; Yu, H.S.; Tischler, B.; Qureshi, M.M.; Soto, J.A.; Anderson, S. Using texture analyses of contrast enhanced CT to assess hepatic fibrosis. *Eur. J. Radiol.* **2016**, *85*, 511–517. [CrossRef]
127. Acharya, U.R.; Ng, E.Y.; Tan, J.-H.; Sree, S.V.; Ng, K.-H. An integrated index for the identification of diabetic retinopathy stages using texture parameters. *J. Med. Syst.* **2011**, *36*, 2011–2020. [CrossRef] [PubMed]
128. Gentillon, H.; Stefańczyk, L.; Strzelecki, M.; Respondek-Liberska, M. Parameter set for computer-assisted texture analysis of fetal brain. *BMC Res. Notes* **2016**, *9*, 496. [CrossRef] [PubMed]
129. Szczypiński, P.M.; Strzelecki, M.; Materka, A.; Klepaczko, A. Mazda—A software package for image texture analysis. *Comput. Methods Programs Biomed.* **2009**, *94*, 66–76. [CrossRef] [PubMed]
130. Ilyasova, N.; Demin, N.; Shirokanev, A.; Paringer, R. Fundus image segmentation using decision trees. In Proceedings of the 2020 International Conference on Information Technology and Nanotechnology (ITNT), Samara, Russia, 26–29 May 2020; pp. 1–6.
131. Ilyasova, N.Y.; Shikhevich, V.A.; Shirokanev, A.S. CUDA parallel programming technology application for analysis of big biomedical data based on computation of effectiveness features. *J. Phys. Conf. Ser.* **2019**, *1368*, 052006. [CrossRef]
132. Ilyasova, N.; Shirokanev, A.; Klimov, I.; Paringer, R. Convolutional neural network application for analysis of Fundus Images. In *International Conference on Intelligent Information Technologies for Industry*; Springer: Cham, Switzerland, 2019; pp. 60–67.
133. Ilyasova, N.Y.; Demin, N.S.; Shirokanev, A.S.; Kupriyanov, A.V.; Zamytskiy, E.A. Method for selection macular edema region using optical coherence tomography data. *Comput. Opt.* **2020**, *44*, 250–258. [CrossRef]
134. Andriyanov, N.; Dementyiev, V. Determination of borders between objects on satellite images using a two-proof doubly stochastic filtration. *J. Phys. Conf. Ser.* **2019**, *1353*, 012006. [CrossRef]
135. Zamytskiy, E.A.; Zolotarev, A.V.; Karlova, E.V.; Ilyasova, N.Y.; Shirokanev, A.S. Comparative quantitative assessment of the placement and intensity of laser spots for treating diabetic macular edema. *Russ. J. Clin. Ophthalmol.* **2021**, *21*, 58–62. [CrossRef]
136. Andriyanov, N.A.; Dementiev, V.E.; Tashlinskii, A.G. Detection of objects in the images: From likelihood relationships towards scalable and efficient neural networks. *Comput. Opt.* **2022**, *46*, 139–159. [CrossRef]
137. Andriyanov, N.A. Analysis of the Acceleration of Neural Networks Inference on Intel Processors Based on OpenVINO Toolkit. In Proceedings of the 2020 Systems of Signal Synchronization, Generating and Processing in Telecommunications (SYNCHROINFO), Svetlogorsk, Russia, 1–3 July 2020; pp. 1–5.

138. Andriyanov, N.; Papakostas, G. Optimization and Benchmarking of Convolutional Networks with Quantization and OpenVINO in Baggage Image Recognition. In Proceedings of the 2022 VIII International Conference on Information Technology and Nanotechnology (ITNT), Samara, Russia, 23–27 May 2022; pp. 1–4.
139. Andriyanov, N.A.; Dementiev, V.E.; Tashlinskiy, A.G. Development of a Productive Transport Detection System Using Convolutional Neural Networks. *Pattern Recognit. Image Anal.* **2022**, *32*, 495–500. [CrossRef]